



Article

A Method for Predicting Landslides Based on Micro-Deformation Monitoring Radar Data

Weixian Tan ^{1,2}, Yadong Wang ^{1,2}, Pingping Huang ^{1,2,*}, Yaolong Qi ^{1,2}, Wei Xu ^{1,2}, Chunming Li ^{1,2} and Yuejuan Chen ^{1,2}

¹ College of Information Engineering, Inner Mongolia University of Technology, Hohhot 010051, China

² Inner Mongolia Key Laboratory of Radar Technology and Application, Hohhot 010051, China

* Correspondence: hwangpp@imut.edu.cn; Tel.: +86-0471-360-1821

Abstract: Mine slope landslides seriously threaten the safety of people's lives and property in mining areas. Landslide prediction is an effective way to reduce losses due to such disasters. In recent years, micro-deformation monitoring radar has been widely used in mine slope landslide monitoring. However, traditional landslide prediction methods are not able to make full use of the diversified monitoring data from these radars. This paper proposes a landslide time prediction method based on the time series monitoring data of micro-deformation monitoring radar. Specifically, deformation displacement, coherence and deformation volume, and the parametric degree of deformation (*DOD*) are calculated and combined with the use of the tangent angle method. Finally, the effectiveness of the method is verified by using measured data of a landslide in a mining area. The experimental results show that our proposed method can be used to identify the characteristics of an imminent sliding slope and landslide in advance, providing monitoring personnel with more reliable landslide prediction results.

Keywords: landslide prediction; deformation monitoring; micro-deformation monitoring radar; coherence



Citation: Tan, W.; Wang, Y.; Huang, P.; Qi, Y.; Xu, W.; Li, C.; Chen, Y. A Method for Predicting Landslides Based on Micro-Deformation Monitoring Radar Data. *Remote Sens.* **2023**, *15*, 826. <https://doi.org/10.3390/rs15030826>

Academic Editors: Constantinos Loupasakis, Ioannis Papoutsis and Konstantinos G. Nikolakopoulos

Received: 4 January 2023

Revised: 29 January 2023

Accepted: 30 January 2023

Published: 1 February 2023



Copyright: © 2023 by the authors. Licensee MDPI, Basel, Switzerland. This article is an open access article distributed under the terms and conditions of the Creative Commons Attribution (CC BY) license (<https://creativecommons.org/licenses/by/4.0/>).

1. Introduction

As one of the most harmful natural disasters in the world, landslides can cause drastic loss of life and property every year [1–4]. In recent years, open-pit mining engineering activities have been expanding on a large scale along with the rapid development of mining technology and the continuous growth in global raw material demand, resulting in a sharp increase in the number of high and steep slopes in mining areas [5–8]. According to incomplete statistics, there are currently 10,100 non-coal metal mines and 73,548 non-metallic mines in China, and from 2001 to 2007, there were 1951 landslide accidents in metal and non-metal open-pit mines, with 3065 casualties [9–12]. The potential safety hazards on the rock slopes of open-pit mines represent the core problem of mine safety production. Accordingly, in 2018, China put forward the idea of “establishing an efficient and scientific natural disaster defense system and improving the ability of the whole society to prevent and control natural disasters” to achieve early identification, monitoring, and early warning of major geological disasters. In the future, organic collaborative means of air–space–ground monitoring will be used to ensure the safe production of mines [13–15].

The slopes of open-pit mining areas are so steep and abrupt that they can be rather dangerous to even observe. Large-scale and long-term real-time monitoring cannot be achieved using traditional slope measurement technologies such as GPS and total station, and it is also difficult to reflect the overall trend of slope deformation [16–21]. With the advancement of science and technology, micro-deformation monitoring radar has been widely used in open-pit mine slope landslide monitoring. It is capable of long-distance and all-weather real-time monitoring, using the phase change of electromagnetic waves to obtain the overall deformation information of the target area. As a result, it has attracted extensive attention

worldwide [22–29]. In addition, coherence of the target deformation area can also be obtained using micro-deformation monitoring radar. A significant difference in the coherence of the target at two different times means that the target has a large deformation. The coherence will be reduced by rainfall, snowfall, and other factors, so good coherence is an important prerequisite for obtaining the deformation value [29–32]. In general, coherence gives an important and valuable reference and implication for deformation.

Since the 1960s, many scholars have carried out a series of studies on landslide prediction, wherein the Saito model, Fukuzono model, and Voight model are typical representatives of creep theory. They are suitable for short-term landslide prediction and temporary slip prediction [33–37] but are limited to gravity-type landslides only. Due to the complex failure mechanism of slopes, nonlinear models such as neural network models and collaborative prediction models always result in differences from the actual slope system [38–40]. In addition, Xu Qiang used the improved tangential angle method as an important indicator in early warning for landslides and achieved good results [41–43]. The existing methods can barely make the best of diverse data obtained by micro-deformation monitoring radar, despite its wide application. So, to take full advantage of these data, there is an urgent need to find a landslide prediction method suitable for micro-deformation monitoring radar.

In addition, the setting of the slope threshold is one of the key steps in landslide prediction. Once the corresponding parameters of a slope exceed the threshold, it is considered to be at risk of collapse. The early warning value is adjusted and continuously optimized in the process of data accumulation and application through the initially set empirical value so as to slowly approach the best early warning threshold applicable to different types of slopes [44]. However, the setting of the early warning value is not static, and there is no absolute universal early warning value. The traditional strategy usually uses a single threshold setting for early warning, which can be susceptible to the environment and other factors, resulting in false early warning.

In summary, based on the time series monitoring data of mine slopes obtained by micro-deformation monitoring radar, the degree of deformation (*DOD*) was calculated in this study by applying parameters such as deformation displacement, coherence, and deformation volume. Then, a comprehensive landslide early warning method combining the multi-threshold criterion and tangent angle was proposed. The effectiveness of the method in realizing early warning of slope landslides is verified through measured data.

2. Study Area

The experimental site, located in the northwest of China, is an open-pit mine on the slope of the low and middle part of the Altai Mountains. The altitude of the open-air stope is 1000–1300 m. The site is 1.2 km long in the northwest–southeast direction and 0.7 km long in the northeast–southwest direction; the terrain is high in the north and low in the east and south, with a relative height difference of 50–300 m; the bedrock slope was formed after the exploitation of the open-pit mine with the destruction of original terrain and landform. Accordingly, multiple platforms with noticeable elevation differences occur, leading to undulating terrain. Figure 1 shows a panorama of the open-pit mine from the radar perspective.

Geologically, the lithology of the study area can be divided into five categories: gneiss, schist, granulite, marble, and amphibolite. The rock mass inside the slope is relatively complete, and the integrity of the rock mass from the surface to the deep part gradually increases, except for the inner part of the slope due to the structural fracture zone caused by fragmentation of the rock mass, whereas the remaining rock masses are relatively complete and hard rock masses.



Figure 1. Open-pit mine slope from the radar perspective.

In this experiment, linear scanning micro-deformation monitoring radar was used for monitoring; the radar operates in the Ku band, with an azimuth resolution of 0.3° and a distance resolution of 0.2 m (Figure 2). The monitoring period was from 0:00 on 18 April 2021 to 10:00 a.m. on 21 April 2021, and a total of 225 radar images were acquired. A radar image obtained by the micro-deformation monitoring radar is shown in Figure 3. Since the monitoring scenes are mostly rock structures with strong scattering, the imaging results are fairly clear.



Figure 2. (a) micro-deformation monitoring radar protection device; (b) micro-deformation monitoring radar.

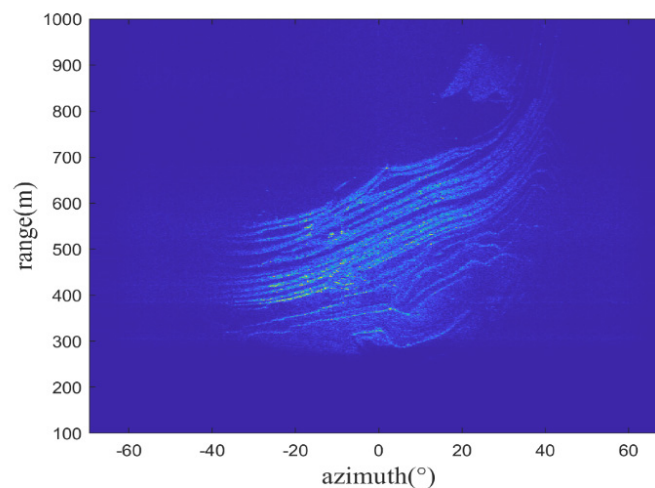


Figure 3. Radar image of monitored scene.

3. Method

In the 1960s, Saito proposed a landslide prediction model based on creep theory after a large number of landslide experiments, as shown in Figure 4, which divides the landslide process into three stages, and slope instability often occurs in the third stage, namely the accelerated deformation stage. In 2009, Xu Qiang proposed the early warning criterion of a tangent angle landslide based on the three-stage evolution characteristics of the Saito model curve, and the dimensions of the longitudinal and horizontal coordinates of the displacement time curve were found to be consistent through coordinate transformation [41,45]; the expression of the improved tangent angle is as follows:

$$\alpha = \arctan(V/V_a) \quad (1)$$

where V is the actual deformation rate of the landslide and V_a is the deformation rate of the uniform speed deformation stage of the landslide. When the tangent angle is greater than 45° , it marks the beginning of the landslide in the accelerated deformation stage, and the closer the tangent angle is to 90° , the closer the occurrence of a landslide (Figure 5).

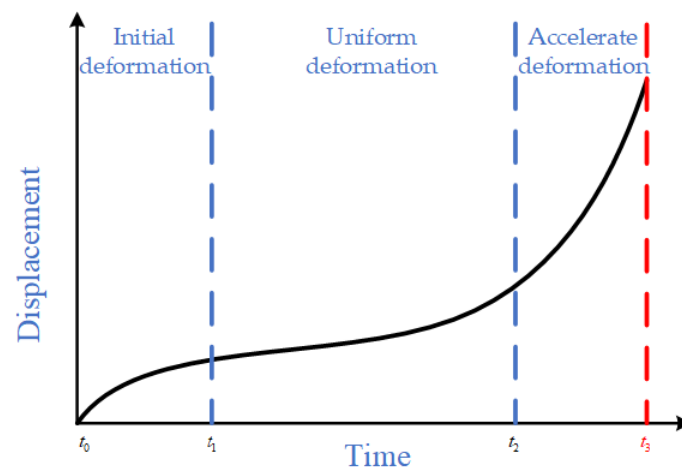


Figure 4. Saito curve model.

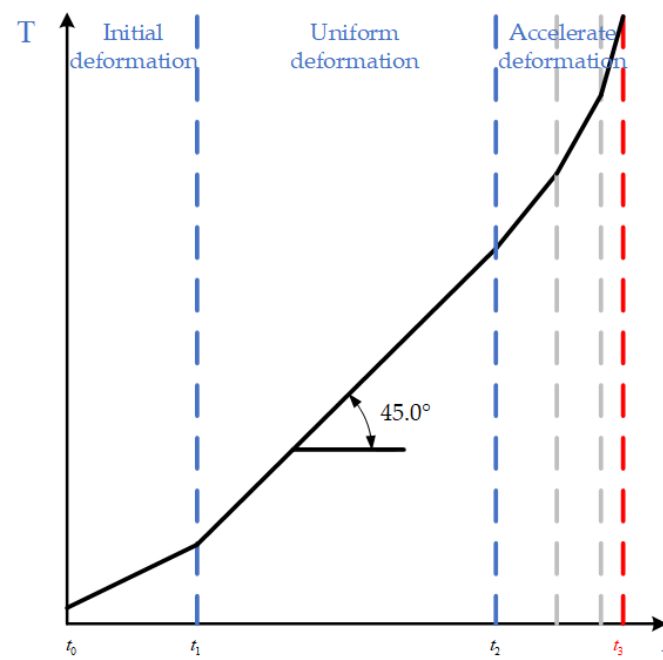


Figure 5. Tangent angle model.

3.1. Forecast Process

The flow chart of slope landslide prediction proposed in this paper is shown in Figure 6. First, all pixels of radar data are traversed, and deformed pixels are filtered out according to the cumulative deformation displacement threshold and deformation velocity threshold. Then, the filtered pixels are then connected by a connectivity algorithm to obtain multiple connected areas. When the deformation area is determined, the *DOD* (degree of deformation) of the target area is obtained by calculating the area, volume, and average coherence of the deformation area. Finally, the new tangent angle warning criterion is used in landslide prediction.

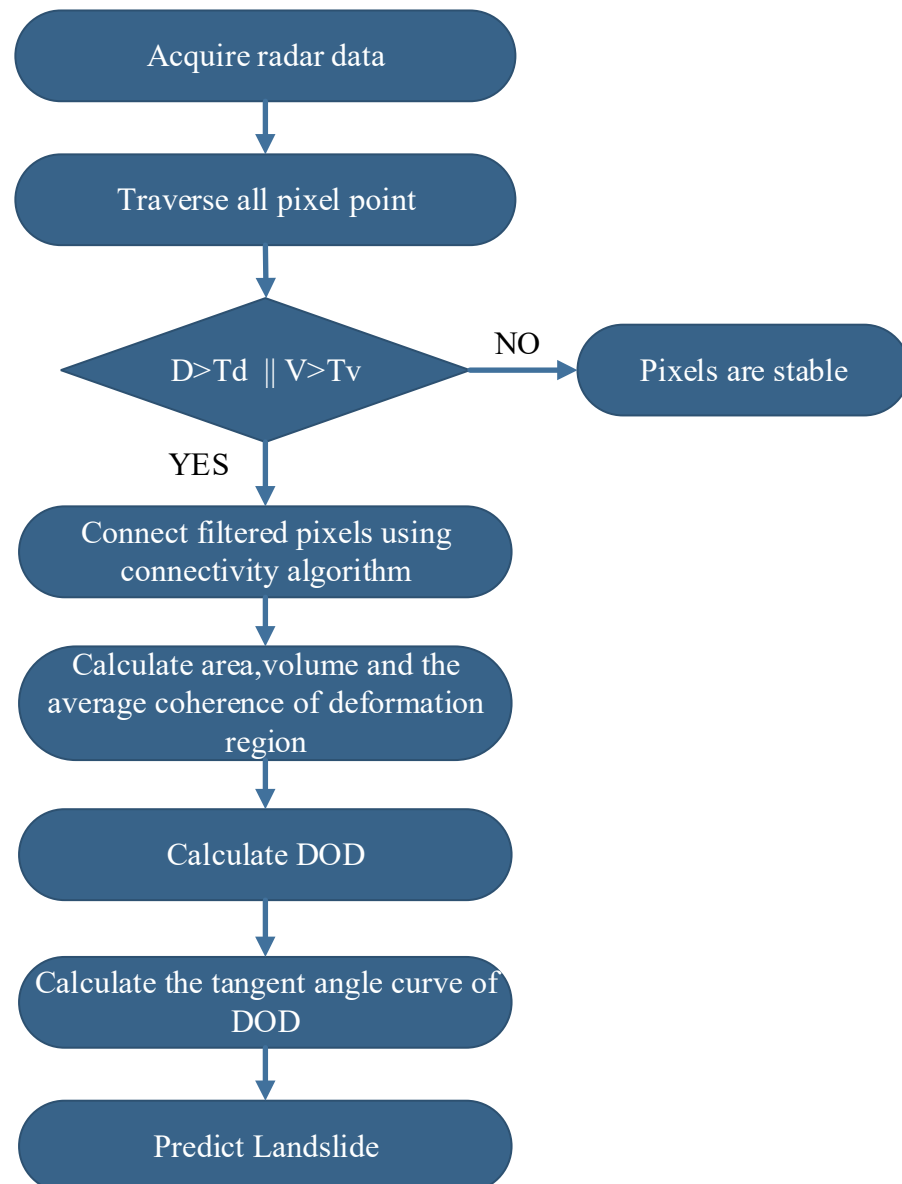


Figure 6. Flowchart of the landslide prediction method.

3.2. *DOD*

The azimuth resolution of the micro-deformation monitoring radar is expressed by the azimuth, which leads to an uneven size for the actual terrain corresponding to each pixel of the radar data. The farther the distance, the larger the pixel area. The pixel area can

be calculated by the azimuth resolution, range resolution, and range sampling position of the micro-deformation monitoring radar [30]:

$$S_{single} = \frac{\alpha}{2} \left([n\beta + R]^2 - [(n-1)\beta + R]^2 \right) = \alpha n\beta^2 + \alpha\beta R - \frac{\alpha}{2}\beta^2 \quad (2)$$

where S_{single} is the area of a single pixel, α is the azimuth resolution, β is the range resolution, n is the sampling position of the corresponding pixel in the range direction, and R is the radar monitoring close distance.

During the long-term monitoring process, the data may fluctuate due to certain uncontrollable factors in the monitoring environment, such as human activities, local vibrations caused by construction, and the noise of the system itself. If only a single pixel is used for region identification, pixels that fluctuate in value due to interference are mistaken for distorted pixels. Landslides, on the other hand, usually require a large deformation area to a certain extent and not just a few isolated pixels. In this paper, pixels are filtered according to the deformation velocity threshold T_v and cumulative displacement threshold T_d . The identified pixels are connected through the connectivity algorithm to identify the sensitive areas that need to be focused on. The landslide warning under multiple thresholds can have a good effect and avoid single-point false warnings. Not only should the actual situation of the monitoring site, including the influence of topography, landform, and human factors, be considered for the setting of the threshold, but also it needs to be continuously adjusted in the process of data collection. The area of the deformation area is the area of the contained pixels, and the deformation volume is calculated as follows:

$$B_v = \sum_{n=1}^N \left(D_{defo,n} \times S_n \right) \quad (3)$$

where B_v is the deformation volume, $D_{defo,n}$ is the deformation value corresponding to the n^{th} pixel, S_n is the area of the n^{th} pixel, and N is the total number of pixels in the deformation area.

The micro-deformation monitoring radar can obtain the coherence of the target, which is the similarity of the observation results of the target at two different times [46]. If the target does not change between two echoes, the target coherence is 1. If the coherence reaches 0, the target is completely incoherent. When the wavelength, angle of incidence, and time baseline of the radar are constant, there is a nonlinear inverse relationship between the deformation velocity and the coherence [32,47]. Qi Lin also demonstrated this conclusion through simulation [30]. The coherence is calculated as follows:

$$\gamma = \left| \frac{\sum_{i=1}^n A_i^2 A_{1,i} \exp\left(i \left[-\frac{4\pi}{\lambda} \Delta R + \Delta\beta\right]\right)}{\sqrt{\sum_{i=1}^n |A_i|^2 * \sum_{i=1}^n |A_i A_{1,i}|^2}} \right| \quad (4)$$

where γ is the coherence, A is the backscattering coefficient of the target, ΔR is the deformation value of the target, and $\Delta\beta$ is the scattering phase. Therefore, the average coherence of the deformation region is as follows:

$$\gamma_{average} = \left(\sum_{n=1}^N \gamma_{average} \right) / N \quad (5)$$

where $\gamma_{average}$ is the average coherence of the deformation region and N is the number of pixels in the deformation region.

Traditionally, the landslide is usually predicted according to a single pixel which can be easily disturbed by environmental factors during monitoring. Thus, the deformation value may be abrupt, leading to misjudgment of the situation of the slope in monitoring.

Therefore, from the point of view of slope, this paper proposes the parameter *DOD* for slope landslide prediction by using the nonlinear inverse relationship between deformation velocity and coherence. To describe the degree of deformation of the slope over a certain period of time, the *DOD* is calculated as follows:

$$DOD = \frac{B_v}{\gamma_{average}^2} \quad (6)$$

The variables used in the calculation of the *DOD* parameter presented in this paper are coherence and deformation volume, but the variables used in the displacement tangent angle method are displacement, so the variables used in the two methods are completely different. By applying the displacement tangent angle method, the diverse data obtained by micro-deformation monitoring radar could not be fully analyzed and studied. Therefore, the newly proposed method, *DOD* tangent angle, is in an attempt to improve this problem. In the actual monitoring process, multiple thresholds and *DOD* tangent angles are used to recognize which stage of accelerated deformation the landslide is currently in so that the landslide can be accurately predicted before it happens.

In summary, this paper proposes a landslide prediction method combining a multi-threshold criterion and the tangent angle, which provides a feasible method for the early warning of open-pit landslides. For a deformed mine slope, as the deformation accumulates, the calculated *DOD* begins to increase, and when the *DOD* increases to a certain extent, a landslide will occur. Usually, before the landslide, the *DOD* curve will increase significantly.

4. Result

The cumulative deformation displacement map within the time window of 0:00 on 18 April 2021 to 9:00 on 21 April 2021 is shown in Figure 7, and it can be clearly seen that the deformation value of pixels in region 1 changes greatly. The pixels are filtered according to the conditional threshold proposed in this article, and the obtained results are shown in Figure 8, where it is obvious that regions 1 and 2 are in the same position in the observation scene, and most of the pixels in region 1 are identified.

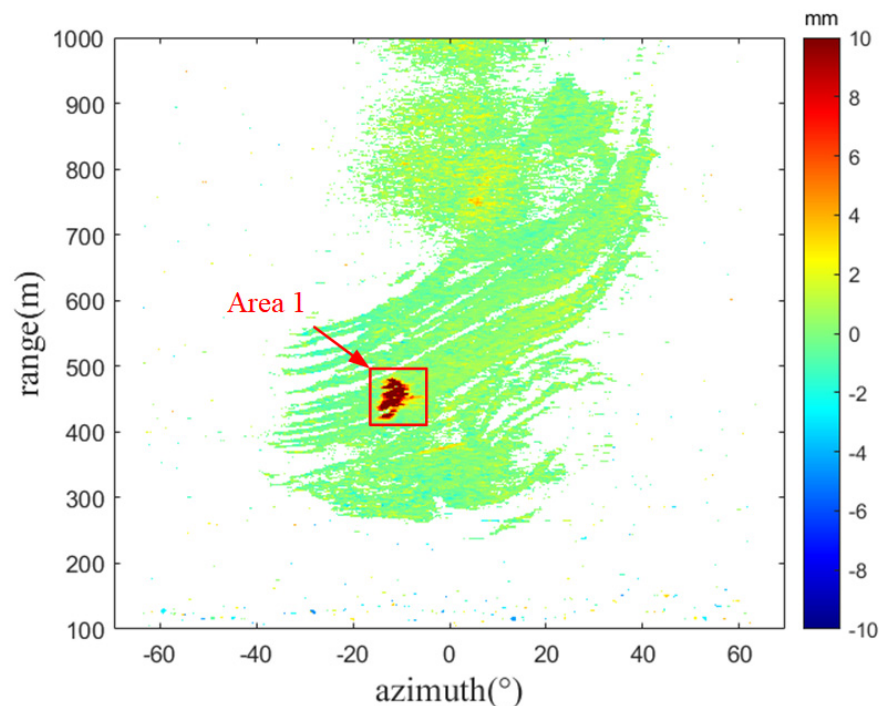


Figure 7. Cumulative deformation diagram.

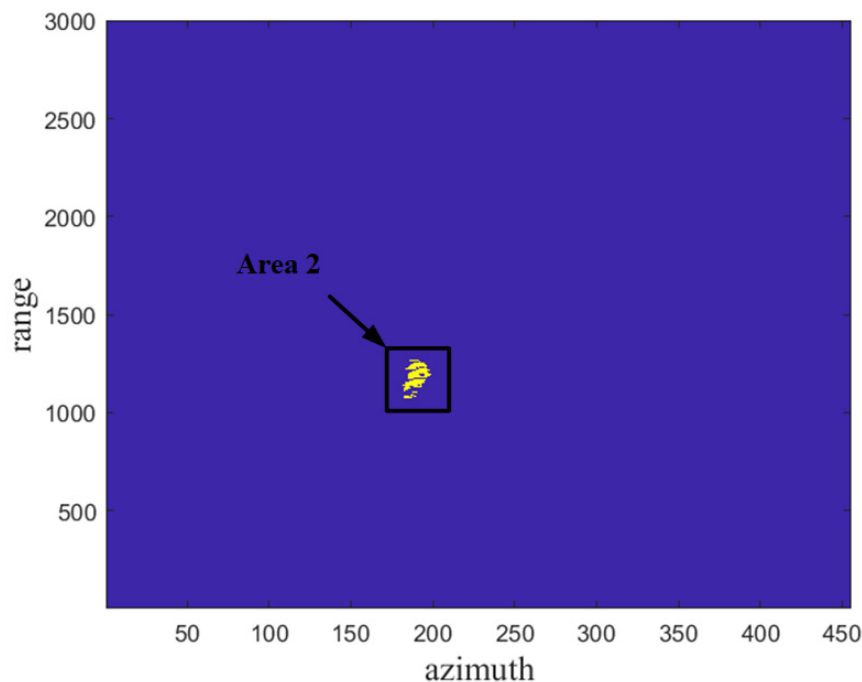


Figure 8. The deformed pixels are finally selected.

It can be seen from Figure 9 that the displacement in the monitoring area is continuously increasing, and the cumulative displacement curve basically conforms to the “three stages” of the Saito model landslide. From 22:54 on 18 April to about 2:00 on 19 April, the region was basically in a stable state without obvious deformation; from 3:00 on 19 April to around 19:00 on 20 April, the deformation in this area is in the stage of constant velocity deformation; from 19:00 on 20 April to around 8:50 on 21 April, the deformation in this area is in the accelerated deformation stage. The cumulative displacement of characteristic points increases sharply, and the deformation speed also continuously increases. The maximum cumulative displacement is 57 mm, and the maximum speed is 10.1 mm/h (Figure 10).

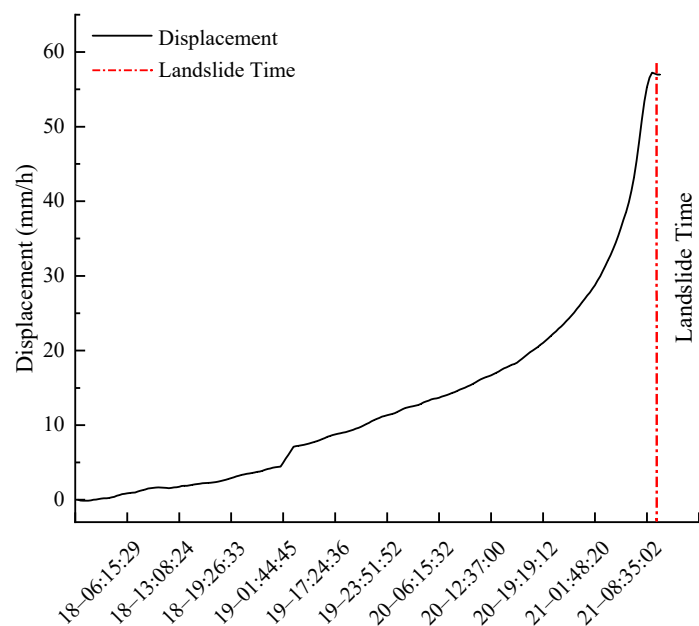


Figure 9. Displacement curve.

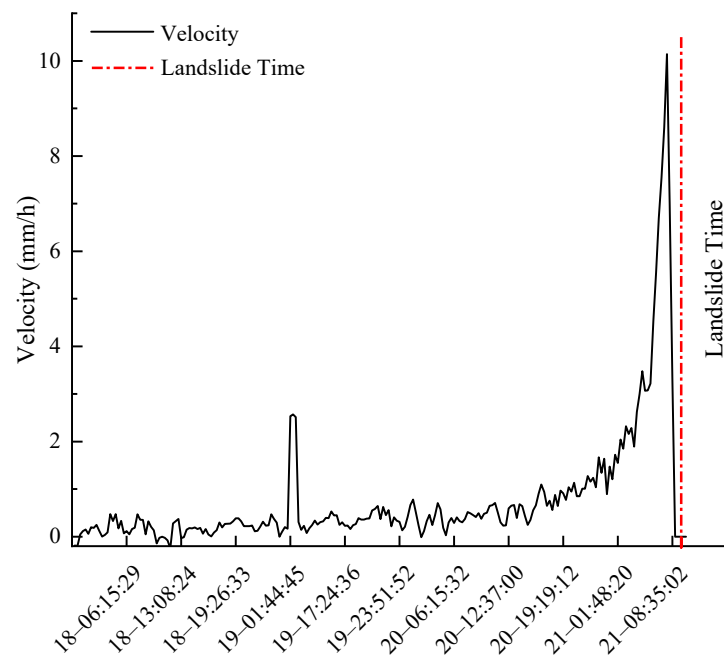


Figure 10. Velocity curve.

The displacement curve before sliding shows a horizontal trend, and the velocity curve shows a downward trend. Owing to rapid deformation, the significantly reduced coherence of the target region makes it impossible for the system to obtain valid deformation data (Figures 9 and 10). As shown in Figure 11, the coherence curve began to decrease overall on the morning of 20 April, and at about 8 a.m. on 21 April, coherence was less than 0.7 and began to drop sharply (based on monitoring experience, the threshold for coherence is usually 0.7). Changes in coherence before landslides provide us with a new perspective for monitoring slopes. Therefore, as shown in Figure 12, the change in coherence is added to the calculation not only to reproduce the deformation trend of the landslide area, but also for comparison with the velocity curve. The *DOD* curve is more concise and clear, and the starting point of rapid growth in *DOD* corresponds to the accelerated deformation stage in the Saito model. *DOD* increases sharply before slippage, and *DOD* obtains the maximum as the landslide occurs. After sliding, *DOD* continues to drop; then, there is a gradual stabilization of the target area and a gradual increase in coherence, and *DOD* continues to decrease. In summary, it is clear that the *DOD* curve reflects the overall trend of the slope in the accelerated deformation stage.

The most critical point of displacement tangent angle determination is the need to determine the uniform speed deformation stage of the displacement–time curve. Because of the interference from environmental factors and measurement errors, the deformation rate at each moment in the constant velocity deformation stage will fluctuate rapidly or slowly, thereby causing difficulties in determining the rate of the uniform speed deformation stage. Therefore, it should be continuously adjusted in line with the actual deformation (Figure 13). The calculation of the value for the parameter *DOD* proposed in this paper begins when the cumulative displacement and the deformation rate reach a certain threshold, at which the slope of the *DOD* curve shows great changes within a relatively short time window. The time window of the uniform deformation stage of *DOD* is narrower, making it easier to obtain the uniform deformation rate of *DOD* compared with the displacement rate. As can be seen from Figure 14, the *DOD* tangent angle curve is more intuitive and clear, the maximum tangent angle is reached at the slip moment, and the displacement tangent angle is determined by the fluctuation of the data. Although there seems to be an overall trend of a gradual increase in the tangent angle, the up and down fluctuations in the actual monitoring process make it easy to make misjudgments in monitoring.

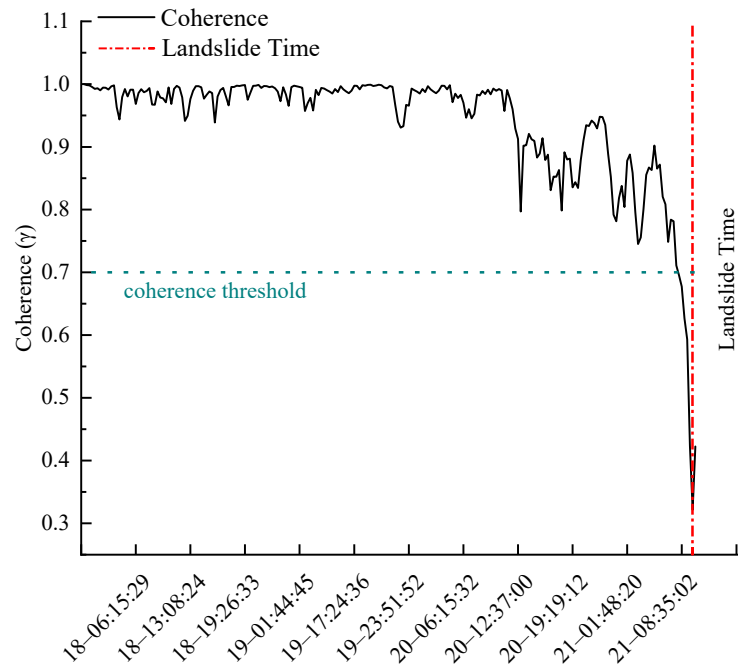


Figure 11. Coherence curve.

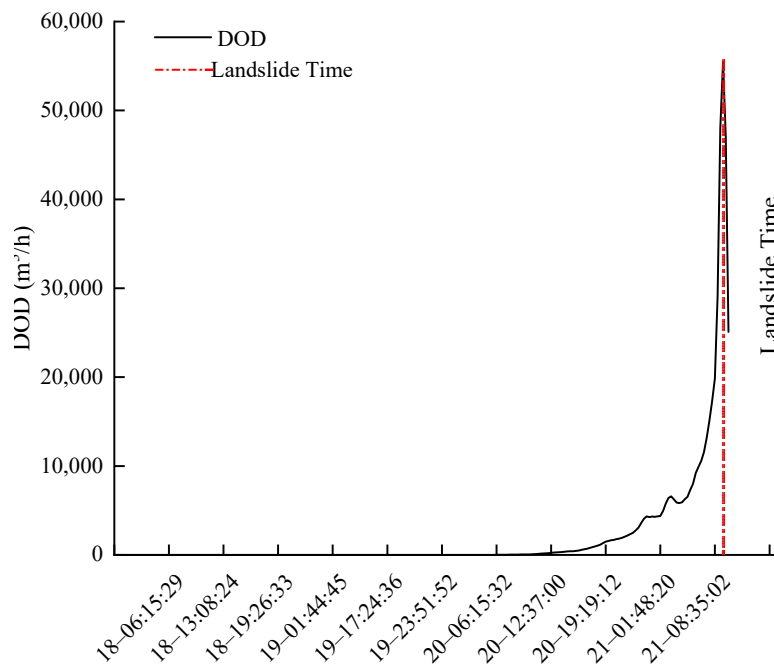


Figure 12. DOD curve.

Landslide prediction can be divided into medium and long-term prediction (more than 6–12 months), short-term prediction (3–6 months), and imminent sliding prediction. Generally, for a mine, prediction 2 h in advance is required. In addition, the instability of slope rock mass is unavoidable. On the premise of not affecting production, the mine will pursue the steepest slope angle with maximum benefit [11]. In summary, in order to more accurately judge the slippage trend of the slope, the velocity threshold, cumulative displacement threshold, and *DOD* tangent angle threshold of different deformation stages before the slope slippage of the open-pit mine were established based on the historical data of the previous slope landslide and the diversified data of the micro-deformation monitoring radar. In addition, a comprehensive early warning criterion, as shown in Table 1,

was established. The acceleration is divided into three stages: the initial acceleration stage is a blue warning, the medium acceleration stage is an orange caution, and the critical sliding stage is a red alarm.

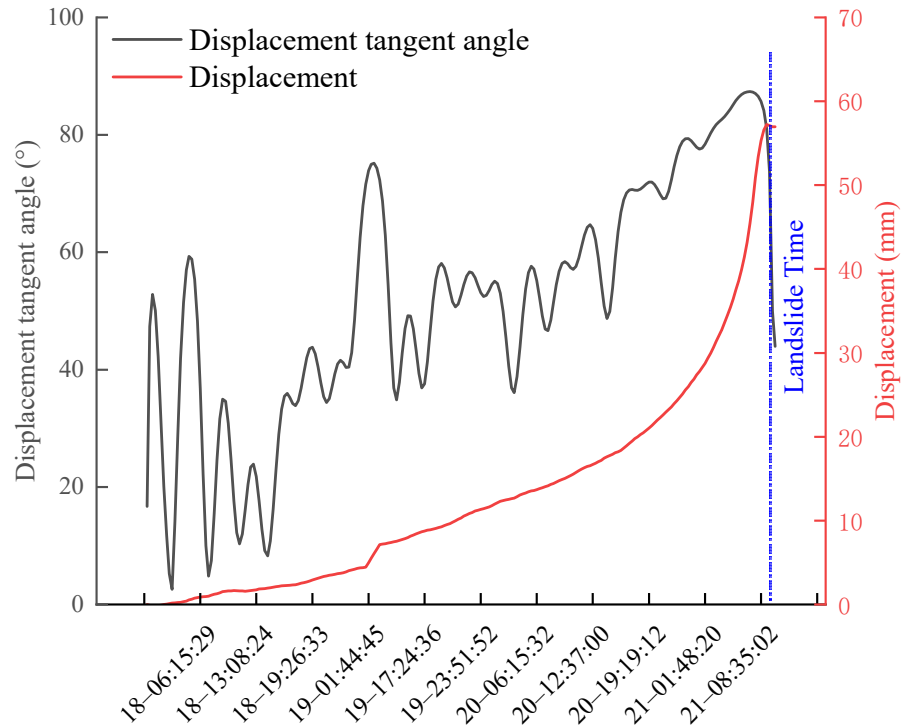


Figure 13. Displacement tangent angle.

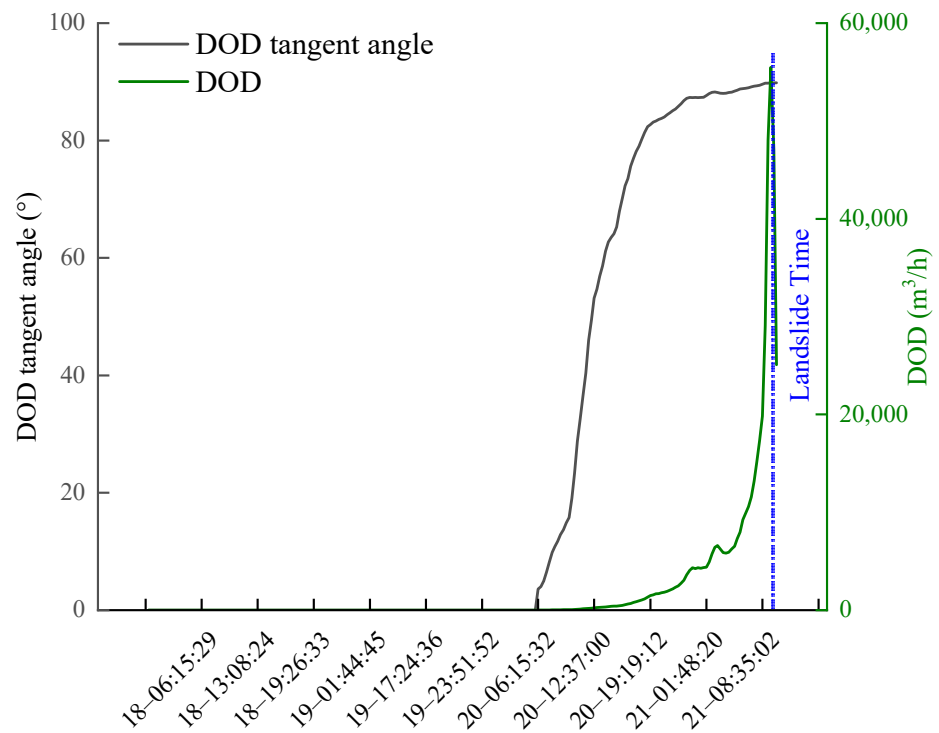


Figure 14. DOD tangent angle.

Table 1. Comprehensive early warning criterion at an accelerated stage.

Deformation Stage	Initial Acceleration	Medium Acceleration	Critical Sliding
Deformation velocity, V (mm/h)	$V > 0.5$	$2 < V < 0.5$	$V > 3$
Cumulative displacement, D (mm/day)	$D > 15$	$14 < D < 30$	$D > 30$
DOD tangent angle, α	$70^\circ < \alpha < 85^\circ$	$85^\circ \leq \alpha < 89^\circ$	$\alpha \geq 89^\circ$
Warning level	Warning	Caution	Alarm

According to the landslide warning criterion proposed in this paper, the fractal deformation rate of 7:05 a.m. on 21 April 2021 was 7.5 mm/h, the cumulative deformation displacement was 47.9 mm, and the DOD tangent angle reached 89.13° , triggering the red warning, and at about 9:37 a.m. on 21 April 2021, the landslide was unstable, and the surveillance video of the mining area recorded the moment of the landslide (Figures 14 and 15). The displacement tangent angle criterion is that when the slope enters the slippery stage, the tangent angle is greater than 85° , and the corresponding moment is 04:45 a.m. on 21 April 2021 (Figures 12 and 13). Complying with the management requirements of the open-pit mine slope, the DOD tangent angle can give a red alarm 2 h in advance so that the mining area is insusceptible. Meanwhile, time is sufficient to transfer the mining facilities from the dangerous area in order to avoid the loss of property and casualties to the maximum extent. The scene after the landslide is shown in Figure 16.

**Figure 15.** Landslide collapse process.**Figure 16.** The scene after the landslide.

The deformation process of the landslide area is shown in Figure 17. The deformation data from radar monitoring are combined with the digital terrain model (DSM) data such that the monitoring personnel can judge the large deformation in the monitoring area by

observing the displacement and deformation cloud map and further improve the accuracy of landslide monitoring in combination with the slope landslide early warning system, greatly improving the effect of landslide prevention.

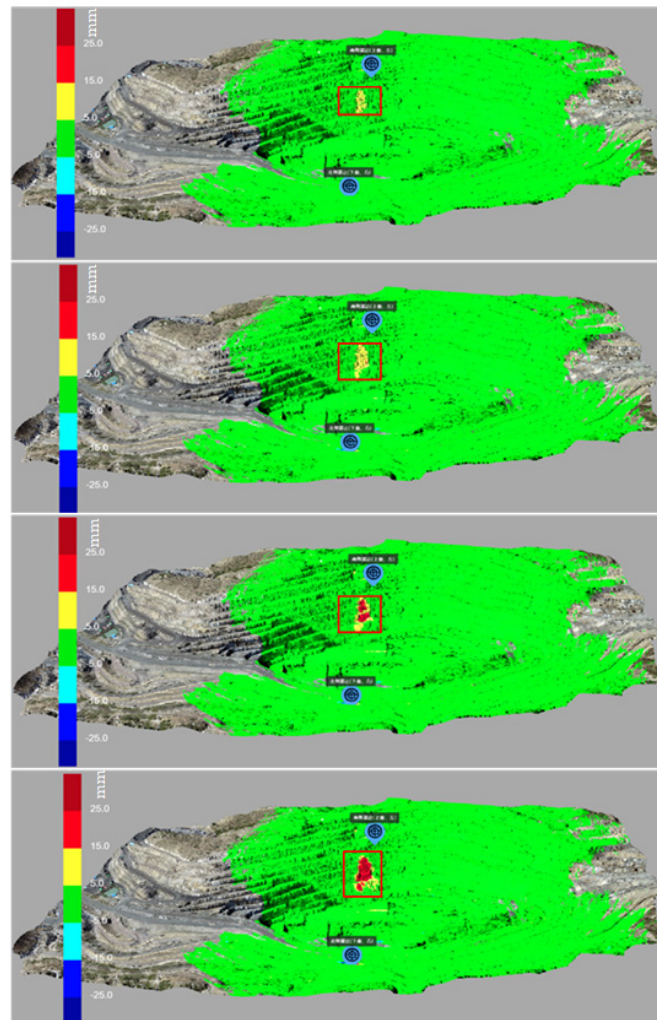


Figure 17. Slope radar monitoring cumulative deformation.

5. Discussion

The traditional threshold early warning strategy is usually used to set the threshold value of a single pixel point for early warning. This is not an ideal situation, because a single pixel point is vulnerable to interference from the external environment and other factors, resulting in the phenomenon of the monitoring data of a single pixel point having a sudden change or continuing to increase. Therefore, when the change in the monitoring data of only a single pixel point is used as the evaluation standard for landslide early warning, it is prone to false early warning. Using remote sensing monitoring means, monitoring is conducted in point cloud monitoring mode. At present, there is less research on the mode of landslide early warning based on the regional surface. Therefore, from the point of view of landslide surface and landslide mass, this paper proposes a landslide early warning index based on double thresholds of deformation velocity and cumulative displacement combined with the tangent angle model to propose a comprehensive early warning criterion for open-pit mine slope landslides.

The setting of a slope threshold is always a difficult problem, and few scholars have proposed effective thresholds. Therefore, the identification of rapidly growing data points is based on a set threshold, which is based on the analysis after a period of data accumulation and needs to be continuously optimized and adjusted in the process of gradual data

collection and enrichment. This value varies for slopes of differing scales, formation conditions, and rock and soil types. The historical data analysis method is used in actual monitoring; it involves judging the maximum deformation rate in the past, which is used as the threshold for an unacceptable maximum deformation rate resulting in a landslide. When setting the actual threshold, according to an actual situation, there should be comprehensive consideration of the nature of rock and soil mass, the degree of artificial disturbance, the possible influence range, and other factors that increase the maximum deformation value by 10–20%. When the slope deformation speed exceeds this value at a certain time, it is necessary to focus on slope stability. If there is no landslide or signs of a landslide, the threshold value is updated according to the deformation speed at this time.

Based on the nonlinear inverse relationship between deformation volume and coherence, a new tangent angle early warning criterion is proposed according to monitoring experience. The target deformation will affect the scattering characteristics of the target. Similarly, weather factors such as rain and snow will also affect the radar echo. Ensuring good coherence is a prerequisite for accurate early warning. Added to that, it should be noted that *DOD* will be calculated only when the deformation speed and cumulative displacement reach a certain cumulative level. Accurate identification of the acceleration phase of the landslide requires substantial data accumulation and analysis.

6. Conclusions

The stability of high and large rock slopes in open-pit mines represents the core problem of safety production in open-pit mines, and the security of open-pit mines in China is still a serious issue. Micro-deformation monitoring radar is widely used in slope monitoring based on its characteristics of high spatial resolution, short time baseline, submillimeter monitoring accuracy, surface monitoring, and suitability for all-weather monitoring. In this paper, a new parameter, *DOD*, is proposed for measuring the degree of slope deformation based on the deformation volume and coherence value, and the tangent angle value of this parameter is combined with the dual threshold values of velocity and displacement in landslide prediction. With the introduction of deformation volume and coherence, this method can be used to provide timely and effective early warning before the sliding of a target and more accurate and reasonable prediction results for slope managers. Based on the measured data of a slope and landslide in a mining area, the method realizes timely warning of an impending landslide and allows the avoidance of property loss in the mining area.

Author Contributions: Conceptualization, W.T.; writing—original draft, Y.W.; methodology, W.T., Y.W. and Y.Q.; formal analysis, Y.W., P.H. and W.X.; supervision, P.H., C.L. and Y.C. All authors have read and agreed to the published version of the manuscript.

Funding: This work was supported in part by the National Natural Science Foundation of China (Grant Nos. 61971246 and 52064039), the Joint Funds of the National Natural Science Foundation of China (Grant No. U22A2010), the Science and Technology Planned Project of Inner Mongolia (Grant Nos. 2019GG139 and 2020GG0073), the Science and Technology Major Project of Inner Mongolia (Grant No. 2019ZD022), the Science and Technology Leading Talent Team of Inner Mongolia (Grant No. 2022LJRC0002), the Fundamental Research Funds for Universities of Inner Mongolia (Grant No. JY20220077), and the Natural Science Foundation of Inner Mongolia (Grant Nos. 2019MS04004, 2020ZD18 and 2021MS06004).

Data Availability Statement: Not applicable.

Acknowledgments: Many thanks to Inner Mongolia Pattern Technology Co., Ltd., for providing the field-measured data. Thanks to anonymous reviewers for their constructive comments to improve the quality of this paper.

Conflicts of Interest: The authors declare no conflict of interest.

References

1. Haque, U.; da Silva, P.F.; Devoli, G.; Pilz, J.; Zhao, B.; Khaloua, A.; Wilopo, W.; Andersen, P.; Lu, P.; Lee, J. The Human Cost of Global Warming: Deadly Landslides and Their Triggers (1995–2014). *Sci. Total Environ.* **2019**, *682*, 673–684. [\[CrossRef\]](#) [\[PubMed\]](#)
2. Lin, Q.; Wang, Y. Spatial and Temporal Analysis of a Fatal Landslide Inventory in China from 1950 to 2016. *Landslides* **2018**, *15*, 2357–2372. [\[CrossRef\]](#)
3. Ma, G.; Hu, X.; Yin, Y.; Luo, G.; Pan, Y. Failure Mechanisms and Development of Catastrophic Rockslides Triggered by Precipitation and Open-Pit Mining in Emei, Sichuan, China. *Landslides* **2018**, *15*, 1401–1414. [\[CrossRef\]](#)
4. Thiebes, B.; Bell, R.; Glade, T.; Jäger, S.; Mayer, J.; Anderson, M.; Holcombe, L. Integration of a Limit-Equilibrium Model into a Landslide Early Warning System. *Landslides* **2014**, *11*, 859–875. [\[CrossRef\]](#)
5. Whittle, D.; Brazil, M.; Grossman, P.A.; Rubinstein, J.H.; Thomas, D.A. Combined Optimisation of an Open-Pit Mine Outline and the Transition Depth to Underground Mining. *Eur. J. Oper. Res.* **2018**, *268*, 624–634. [\[CrossRef\]](#)
6. Amini, M. Stability Analysis of the North-Eastern Slope of Daralou Copper Open Pit Mine against a Secondary Toppling Failure. *Eng. Geol.* **2019**, *249*, 89–101. [\[CrossRef\]](#)
7. Obregon, C.; Mitri, H. Probabilistic Approach for Open Pit Bench Slope Stability Analysis—A Mine Case Study. *Int. J. Min. Sci. Technol.* **2019**, *29*, 629–640. [\[CrossRef\]](#)
8. Song, D.; Che, A.; Zhu, R.; Ge, X. Dynamic Response Characteristics of a Rock Slope with Discontinuous Joints under the Combined Action of Earthquakes and Rapid Water Drawdown. *Landslides* **2018**, *15*, 1109–1125. [\[CrossRef\]](#)
9. Wang, Y.; Zhang, N.N.; Sun, Z.; Fei, W. The major domestic natural disasters in 2017. *Disaster Reduct. China* **2018**, *5*, 38–41.
10. Tian, H.; Bai, R.; Zhao, H. Achievement and developing trend of open-pit mining in China. *Opencast Min. Technol.* **2019**, *34*, 1–9.
11. Yang, T.; Wang, H.; Dong, X. Current situation problems and countermeasures of intelligent evaluation of slope stability in open pit. *J. China Coal Soc.* **2020**, *45*, 2277–2295.
12. Jiao, R.; Wang, S.; Yang, H.; Guo, X.; Han, J.; Pei, X.; Yan, C. Comprehensive Remote Sensing Technology for Monitoring Landslide Hazards and Disaster Chain in the Xishan Mining Area of Beijing. *Remote Sens.* **2022**, *14*, 4695. [\[CrossRef\]](#)
13. Ge, D.; Dai, K.; Guo, Z.; Li, Z. Early Identification of Serious Geological Hazards with Integrated Remote Sensing Technologies: Thoughts and Recommendations. *Geomat. Inf. Sci. Wuhan Univ.* **2019**, *44*, 996–1007.
14. Xu, Q.; Dong, X.J.; Li, W.L. Integrated space-air-ground early detection, monitoring and warning system for potential catastrophic geohazards. *Geomat. Inf. Sci. Wuhan Univ.* **2019**, *44*, 957–966.
15. Li, Z.H.; Song, C.; Yu, C. Application of satellite radar remote sensing to landslide detection and monitoring: Challenges and solutions. *Geomat. Inf. Sci. Wuhan Univ.* **2019**, *44*, 967–979.
16. Qin, H.; Ma, H.; Yu, Z. Analysis Method of Landslide Early Warning and Prediction Supported by Ground-Based SAR Technology. *Geomat. Inf. Sci. Wuhan Univ.* **2020**, *45*, 1697–1706.
17. Bozzano, F.; Mazzanti, P.; Prestininzi, A.; Scarascia Mugnozza, G. Research and development of advanced technologies for landslide hazard analysis in Italy. *Landslides* **2010**, *7*, 381–385. [\[CrossRef\]](#)
18. Intrieri, E.; Gigli, G.; Casagli, N.; Nadim, F. Brief communication “landslide early warning system: Toolbox and general concepts”. *Nat. Hazards Earth Syst. Sci.* **2013**, *13*, 85–90. [\[CrossRef\]](#)
19. Tommaso, C.; Paolo, F.; Emanuele, I.; Kostas, B.; Nicola, C. On the monitoring and early-warning of brittle slope failures in hard rock masses: Examples from an open-pit mine. *Eng. Geol.* **2017**, *228*, 71–81.
20. Lopez-Vinielles, J.; Ezquerro, P.; Fernandez-Merodo, J. Remote analysis of an open-pit slope failure: Las Cruces case study, Spain. *Landslides* **2020**, *17*, 2173–2188. [\[CrossRef\]](#)
21. Carlà, T.; Intrieri, E.; Raspini, F.; Bardi, F.; Farina, P.; Ferretti, A.; Colombo, D.; Novali, F.; Casagli, N. Perspectives on the prediction of catastrophic slope failures from satellite InSAR. *Sci. Rep.* **2019**, *9*, 14137. [\[CrossRef\]](#)
22. Crosetto, M.; Monserrat, O.; Luzi, G.; Cuevas-González, M.; Devanthéry, N. A noninterferometric procedure for deformation measurement using GB-SAR imagery. *IEEE Geosci. Remote Sens. Lett.* **2013**, *11*, 34–38. [\[CrossRef\]](#)
23. Dick, G.J.; Eberhardt, E.; Cabrejo-Liévano, A.G.; Stead, D.; Rose, N.D. Development of an early-warning time-of-failure analysis methodology for open-pit mine slopes utilizing ground-based slope stability radar monitoring data. *Can. Geotech. J.* **2015**, *52*, 515–529. [\[CrossRef\]](#)
24. Zeng, T.; Deng, Y.K. Development state and application examples of ground-based differential interferometric radar. *J. Radars* **2019**, *8*, 154–170.
25. Liu, B.; He, K.; Han, M.; Hu, X.; Ma, G.; Wu, M. Application of UAV and GB-SAR in Mechanism Research and Monitoring of Zhonghaicun Landslide in Southwest China. *Remote Sens.* **2021**, *13*, 1653. [\[CrossRef\]](#)
26. Owerko, T.; Kuras, P.; Ortyl, Ł. Atmospheric Correction Thresholds for Ground-Based Radar Interferometry Deformation Monitoring Estimated Using Time Series Analyses. *Remote Sens.* **2020**, *12*, 2236. [\[CrossRef\]](#)
27. Hu, C.; Deng, Y.; Tian, W.; Zhao, Z. A Compensation Method for a Time-Space Variant Atmospheric Phase Applied to Time-Series GB-SAR Images. *Remote Sens.* **2019**, *11*, 2350. [\[CrossRef\]](#)
28. Huang, Z.; Sun, J.; Tan, W.; Huang, P.; Han, K. Investigation of Wavenumber Domain Imaging Algorithm for Ground-Based Arc Array SAR. *Sensors* **2017**, *17*, 2950. [\[CrossRef\]](#)
29. Gao, H.; Liao, M.; Liu, X.; Xu, W.; Fang, N. Source Geometry and Causes of the 2019 Ms6.0 Changning Earthquake in Sichuan, China Based on InSAR. *Remote Sens.* **2022**, *14*, 2082. [\[CrossRef\]](#)

30. Qi, L.; Tan, W.; Huang, P.; Xu, W.; Qi, Y.; Zhang, M. Landslide Prediction Method Based on a Ground-Based Micro-Deformation Monitoring Radar. *Remote Sens.* **2020**, *12*, 1230. [[CrossRef](#)]
31. Xiao, T.; Huang, W.; Deng, Y.; Tian, W.; Sha, Y. Long-Term and Emergency Monitoring of Zhongbao Landslide Using Space-Borne and Ground-Based InSAR. *Remote Sens.* **2021**, *13*, 1578. [[CrossRef](#)]
32. Zhang, H.; Wang, C. *Research on DInSAR Method Based on Coherent Target*; Science Press: Beijing, China, 2009; pp. 12–28.
33. Zheng, X.; Yang, X.; Ma, H.; Ren, G.; Zhang, K.; Yang, F.; Li, C. Integrated Ground-Based SAR Interferometry, Terrestrial Laser Scanner, and Corner Reflector Deformation Experiments. *Sensors* **2018**, *18*, 4401. [[CrossRef](#)] [[PubMed](#)]
34. Fukuzono, T. A method to predict the time of slope failure caused by rainfall using the inverse number of velocity of surface displacement. *J. Japan Landslide Soci.* **1985**, *2*, 8–13. [[CrossRef](#)]
35. Voight, B. A method for prediction of volcanic eruptions. *Nature* **1988**, *332*, 125–130. [[CrossRef](#)]
36. Zhou, X.; Ye, T. Inverse-Square-Root-Acceleration Method for Predicting the Failure Time of Landslides. *Sci. China Technol. Sci.* **2021**, *64*, 1127–1136. [[CrossRef](#)]
37. Du, J.; Yin, K.; Lacasse, S. Displacement prediction in colluvial landslides, three Gorges reservoir, China. *Landslides* **2013**, *10*, 203–218. [[CrossRef](#)]
38. Du, W.; Wang, G. A one-step Newmark displacement model for probabilistic seismic slope displacement hazard analysis. *Eng. Geol.* **2016**, *205*, 12–23. [[CrossRef](#)]
39. Lian, C.; Zeng, Z.; Yao, W.; Tang, H. Multiple neural networks switched prediction for landslide displacement. *Eng. Geol.* **2015**, *186*, 91–99. [[CrossRef](#)]
40. Chousianitis, K.; Gaudio, V.; Kalogeras, I. Predictive model of Arias intensity and Newmark displacement for regional scale evaluation of earthquake-induced landslide hazard in Greece. *Soil Dyn. Earthq. Eng.* **2014**, *65*, 11–29. [[CrossRef](#)]
41. Xu, Q.; Zeng, Y.; Qian, J.; Wang, C.; He, C. Study on an improved tangential angle and the corresponding landslide pre-warning criteria. *Geol. Bull. China* **2009**, *28*, 501–505.
42. Xu, Q.; Peng, D.; He, C.; Qi, X.; Zhao, K.; Xiu, D. Theory and method of monitoring and early warning for sudden loess landslide—A case study atheifangtai terrace. *J. Eng. Geol.* **2020**, *28*, 111–121.
43. Xu, Q. Understanding the landslide monitoring and early warning: consideration to practical issues. *J. Eng. Geol.* **2020**, *28*, 360–374.
44. Intrieri, E.; Gigli, G.; Mugnai, F.; Fanti, R.; Casagli, N. Design and implementation of a landslide early warning system. *Eng. Geol.* **2012**, *147*, 124–136. [[CrossRef](#)]
45. Wang, J.; Zhang, Z. *System Engineering Geology Study on Typical Rapid Loess Landslides*; Sichuan Science & Technology Press: Chengdu, China, 1999.
46. Touzi, R.; Lopes, A. Coherence estimation for SAR imagery. *IEEE Trans. Geosci. Remote Sens.* **1999**, *37*, 135–149. [[CrossRef](#)]
47. Zebker, H.A.; Villasenor, J. Decorrelation in interferometric radar echoes. *IEEE Trans. Geosci. Remote Sens.* **1992**, *30*, 950–959. [[CrossRef](#)]

Disclaimer/Publisher’s Note: The statements, opinions and data contained in all publications are solely those of the individual author(s) and contributor(s) and not of MDPI and/or the editor(s). MDPI and/or the editor(s) disclaim responsibility for any injury to people or property resulting from any ideas, methods, instructions or products referred to in the content.